Detection of foreign bodies flowing in a pipe using longitudinal electric excitation

Niloofar Rezaei
Electrical and Computer Engineering
University of Canterbury
Christchurch, New Zealand
niloofar.rezai@pg.canterbury.ac.nz

Michael Hayes
Electrical and Computer Engineering
University of Canterbury
Christchurch, New Zealand
michael.hayes@canterbury.ac.nz

Bill Heffernan
Electric Power Engineering Centre
University of Canterbury
Christchurch, New Zealand
bill.heffernan@epecentre.ac.nz

***Abstract*—This paper presents an impedance-based sensing method for detecting foreign bodies within a conductive flowing medium in a pipe. The principle behind this work is that foreign bodies have different electrical conductivity compared to the food product in the pipe; therefore, measuring and analyzing the system impedance provides insight into the presence or absence of the object, as well as its characteristics (whether conductive or insulating). An AC excitation voltage at the frequency of 10 kHz is applied across the pipeline, using stainless steel sections as electrodes and sight-glass sections as insulators. The impedance variations caused by foreign objects are detected by measuring the resulting current. To improve accuracy, a coaxial excitation method is used to reduce radiated magnetic fields, and a dual sight-glass setup helps reduce common-mode interference. The method is validated through 3D simulations using COMSOL Multiphysics, showing the potential for real-time detection of foreign objects in liquid food processing.**

***Index Terms*—Impedance sensing, foreign body detection, conductive flowing medium, food industry pipelines**

I. Introduction

Foreign object detection is important for ensuring safety and quality in the food industry, especially in the dairy sector. Contaminants such as metal, plastic, and glass in milk and dairy products pose serious health risks and lower product quality [1]. In 2001, the USDA's Food Safety and Inspection Service (FSIS) introduced the Consumer Complaint Monitoring System (CCMS) to track consumer complaints about foreign objects in food. In 2017, 45% of complaints were related to foreign objects, mostly insects and animal parts, causing injuries such as broken teeth, cuts, and choking, some of which needed medical attention [2]. This shows how important it is to prevent contamination in food products.

Foreign objects in processing equipment can cause damage, leading to costly replacements and increased operational costs. Therefore, early detection helps reduce both equipment damage and food contamination. Technology has made it easier to detect and prevent foreign object contamination. Methods like ultrasonic, X-ray, and imaging technologies offer different benefits depending on industry needs. Ultrasonic inspection is a low-cost, non-intrusive method used in the dairy industry because it does not affect the physical or hygienic properties of food [3]. However, it struggles with thick, uneven, and highly absorbing materials, making full product scanning difficult. Improving transducer design, sensitivity, frequency, and bandwidth can increase accuracy. Hybrid methods, like laser-based ultrasound and machine learning, can further improve detection [4]. Metal detectors are widely used in food processing, especially before packaging, to find metal contaminants. While effective, they do not fully remove the risk of contamination. Metal detectors act as a warning system, but further checks and actions are needed to ensure food safety [2]. They also cannot detect all foreign materials, including glass, plastic, rubber, and natural objects like rocks or seeds. To improve detection, X-ray systems are often used alongside metal detectors for better quality control [5]. X-ray systems can detect foreign objects without damaging food but struggle with materials like paper, plastic, and insects. Advanced X-ray technologies, such as phase contrast and grating-based multi-modal methods, offer better detection [6]. However, X-ray systems still have limits due to production speeds and energy limits of the X-ray source, making them less suitable for thicker products [7].

More advanced imaging methods have recently been introduced for foreign object detection in the food industry. Electrical impedance tomography (EIT) has been used to train a deep learning model for binary classification to identify contaminated samples [8]. EIT methods are widely used in medical applications, as they provide unique physiological data that other monitoring methods cannot [9]. In medical settings, where the object remains stationary, EIT is often sufficient. However, this method is slow because the excitation signal is applied sequentially between electrode pairs. As a result, it is less effective for moving systems, such as pipe flow or fast-moving products, where objects remain in the sensing area only briefly. In such cases, an alternative approach is longitudinal electrical excitation, which detects changes in electromagnetic fields caused by foreign objects [10]. This method enables faster detection but is less effective for imaging.

This paper discusses a simpler impedance-based sensing method using longitudinal excitation. Section II explains the system operation, while Section III details the simulation steps in COMSOL Multiphysics. Section IV describes the experimental setup, followed by both simulation and experimental results in Section V. Section VI discusses the obtained results, and finally, Section VII concludes the paper.

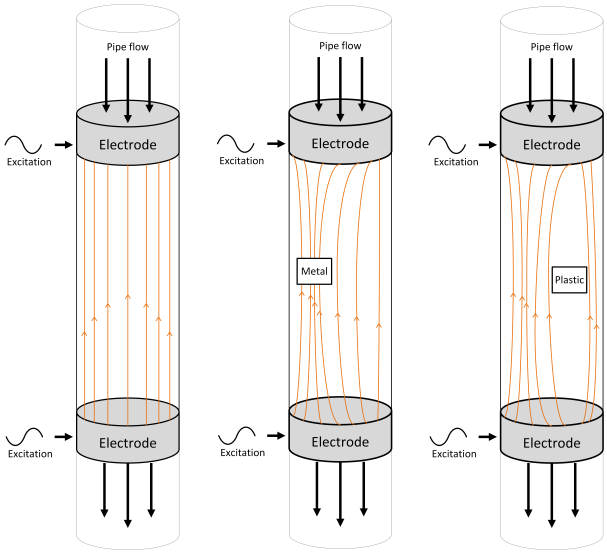

Fig. 1. An example of a bipolar AC longitudinal excitation applied to the contents of a pipe filled with a homogeneous fluid. When no object is present, the current density is uniform across the central section of the pipe. A metallic object increases the local conductivity and an insulating object reduces the local conductivity. This causes the current streamlines to deflect.

II. System operation

The principle behind the operation of the sensor is that foreign bodies have a markedly different electrical conductivity to the food product in a pipe. An AC excitation voltage is applied across the fluid using the stainless-steel pipes as electrodes with a sight-glass (Figure 2) as an insulator between them. The current through the electrodes is sensed using a current transformer, and the impedance is estimated using a synchronous demodulator. Current transformers have been used with suitable amplifiers to provide better precision, cause insignificant voltage drop, and remove any common-mode signals due to their inherent isolation [11]. If there is a foreign body within the food, the current density is no longer homogeneous, and this changes the excitation current and thus the impedance. The current transformers are being used to individually measure the currents in the four return conductors, which are an inherent part of the sight-glass structure. In this fashion, the sight-glass contents behave like a coaxial load and external magnetic field, due to the excitation is cancelled. Although all four currents can be summed and measured with a single current transformer, the circuits are not costly, and if higher frequency excitation than reported here is used, imbalance between the four currents can potentially provide additional information on the location of any foreign object[11].

A four wire Kelvin connection could be used to mitigate the electrode impedance, by injecting an excitation current and sensing the voltage across a second pair of electrodes. However, this increases the complexity of the system. Moreover, since the electrodes are the stainless-steel pipes used to transport food, they have large surface area. This reduces the contact impedance and the power-law noise generated at the electrode-electrolyte interface.

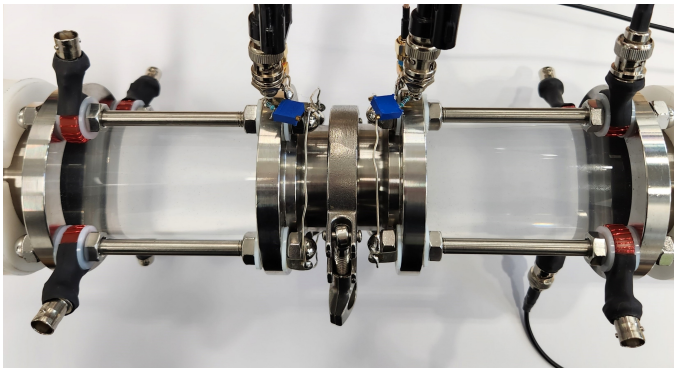

Fig. 2. Photo of a sight-glass impedance sensor. Visible are the four rods (horizontal) used to ensure coaxial excitation. The red coils on each rod are current transformers for sensing the current.

A coaxial excitation is employed to reduce radiated magnetic fields. This is achieved using metal rods for the return current, spaced radially around the sight-glass.

A. Common-mode interference reduction

To reduce common-mode interference, a pair of sight-glasses can be used. These are inserted in series with a separating stainless-steel pipe providing a third electrode. This has the advantage that the stainless-steel pipework outside the sensor can be kept at ground potential.

There are two strategies to reduce the common-mode interference. The simplest is to apply a voltage, as shown in Figure 4, (or current) to the common electrode and measure the excitation current (or voltage). With this configuration, the impedances of the fluid inside the two sight-glasses are in parallel. This helps to reduce magnetically coupled interference.

A second approach is to use a pair of sources, as shown in Figure 5, and calculate the difference in measured current (or voltage). Here the phasor current from sensor 1 has the form

$$I_1 = \frac{V_x}{Z_1}, \tag{1}$$

where V_x is the excitation voltage (applied to both sensors) and Z_1 is the impedance between the electrodes. Similarly, the current from sensor 2 has the form

$$I_2 = \frac{V_x}{Z_2}. \tag{2}$$

Subtracting the currents helps to reduce capacitively coupled interference. The difference in current between the two sensors is

$$\Delta I = I_2 - I_1 = V_x \left(\frac{1}{Z_2} - \frac{1}{Z_1} \right). \tag{3}$$

With a homogeneous medium, $Z_1 = Z_2 = Z$. However, if an object enters sensor 1, then $Z_2 = Z_1 + \Delta Z$, where ΔZ is the additional impedance due to the object. Similarly, when the object enters sensor 2, then $Z_2 = Z_1 - \Delta Z$.

Insulating foreign bodies can be recognised from conducting foreign bodies, since the impedance goes up for an insulating foreign body and down for a conducting foreign body.

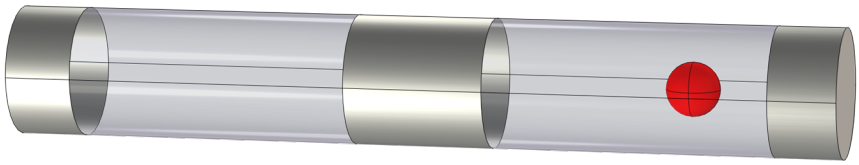

Fig. 3. Dual sensor arrangement. The light coloured regions indicate the sight-glasses and the grey regions indicate stainless-steel electrodes. The red sphere represents a foreign object passing through the first sight glass. The sensor has an internal diameter of 48 mm; each section has a length of 105 mm.

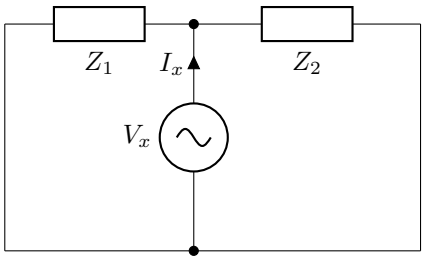

Fig. 4. Electrical schematic of the sensor pair with single excitation.

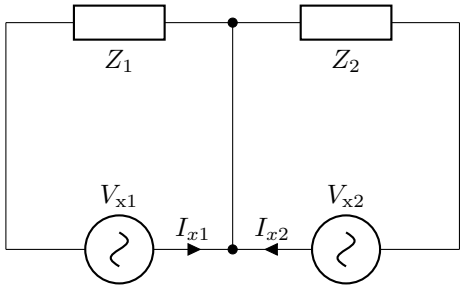

Fig. 5. Electrical schematic of the sensor pair with dual excitation.

B. Current measurement

The excitation currents are measured using current transformers. The transformer secondary current is converted to a voltage using a transimpedance amplifier. An auto-zeroing amplifier is required to keep the voltage across the secondary zero to avoid magnetization [11].

III. Simulation

COMSOL Multiphysics, version 6.2, was used to model the sensing region of a pipeline for foreign object detection. The detection method is based on impedance measurements, comparing them to a baseline value when no object is present.

A. Simulation geometry setup

The simulation geometry consists of stainless steel sections acting as electrodes and glass sections serving as insulators between the stainless steel parts. All components are modelled as cylinders in COMSOL (Figure 3). These cylinders are filled with a conductive fluid, such as milk, and the material properties are provided in Table I.

B. Meshing and computational considerations

To ensure both accuracy and efficiency, it is important to use an appropriate mesh. A finer mesh enhances accuracy by capturing more detailed information. However, it will increase the number of elements, which leads to longer simulation times. In this study, a fine mesh with a minimum element size of 0.1 mm was applied in the fluid domain, and a coarser mesh was used in the surrounding air domain to ensure a balance between accuracy and computational efficiency.

TABLE I
Material Properties Used in the Simulation.

Material	Electrical Conductivity (S/m)	Relative Permittivity	Relative Permeability
Milk	0.5	1	1
Stainless Steel 405	1.73913×10^6	1	1
Glass	1×10^{-14}	4.2	1
Rubber Object	1×10^{-16}	1	1

C. Applied equations and physics

The Electric Current interface in COMSOL was used and the electric field and current density are governed by

$$\nabla \cdot \mathbf{J} = 0, \tag{4}$$

where

$$\mathbf{J} = \sigma \mathbf{E} + \mathrm{j}2\pi f_x \mathbf{D} + \mathbf{J_e}. \tag{5}$$

Here $\mathbf{J}$ is the current density vector, σ is the electrical conductivity, $\mathbf{E}$ is the electric field, $\mathrm{j}2\pi f_x \mathbf{D}$ represents displacement currents for an excitation frequency f_x, and $\mathbf{J_e}$ represents external current sources.

The electric displacement field $\mathbf{D}$ is related to the electric field $\mathbf{E}$ by

$$\mathbf{D} = \epsilon \mathbf{E}, \tag{6}$$

where ϵ is the permitivitty and the electric field $\mathbf{E}$ is related to the electric potential V by:

$$\mathbf{E} = -\nabla V. \tag{7}$$

This assumes that time-changing magnetic fields have negligible effect.

To determine the impedance between the electrodes, an electric current of 1 ampere is applied as a terminal boundary condition to the middle stainless steel cylinder. Three approaches are considered:

1) *Single sensor with single excitation*: When there is one sight glass with two metal cylinders at each end, one of them is excited with 1 ampere current, and the other one is ground.
2) *Dual sensor with single excitation*: The middle metal cylinder is excited with a 1-ampere current, and both

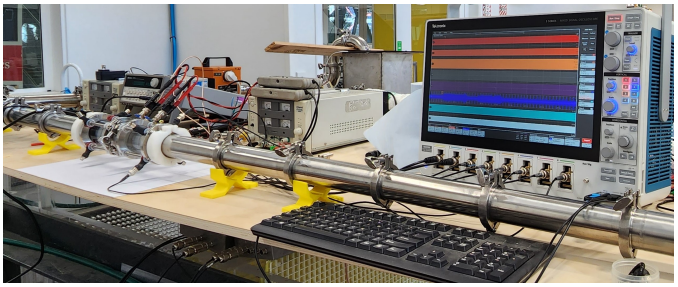

Fig. 6. Photo of the dual sensor installed in the recirculating test rig. The sight-glasses can be seen in the left foreground.

metal side cylinders are grounded simultaneously; therefore, the sight glasses are electrically in parallel.

3) *Dual sensor with dual excitation*: In this configuration, the central cylinder is grounded, and each of the side electrodes is driven by a 1 Amp current. The sight glasses can be considered to be connected in series. However, due to the opposing directions of current flow in each, their respective impedances subtract from each other.

D. Solver configurations and steps

A frequency domain study was conducted at 10 kHz to calculate impedance variations as the object moves through the sight glasses. A parametric sweep was performed to evaluate impedance changes at different positions of the object, moving along the x and z axes. The initial position of the object was $x = 0\,\text{mm}, y = 0, z = -190\,\text{mm}$. It moved longitudinally along the z axis from -190 mm to +190 mm, and radially along the x axis from 0 mm to 10 mm. The step size was 5 mm for both axes. Impedance was calculated for all combinations of x and z positions.

IV. Experiment

The sensor was tested by inserting the sight-glasses into a recirculating rig, see Figure 6. This used a ring of stainless-steel pipework joined with tri-clover clamps. A centrifugal pump provided the fluid flow. Foreign objects were introduced using a pair of valves in an air-lock arrangement and removed before the pump with a filter.

A dual sight-glass system with single excitation was employed, with a 10 kHz AC excitation provided by a HP 33120A signal generator. The signals were recorded with a Tektronix MSO58B oscilloscope connected to custom current probes and Keysight N2791A differential voltage probes. The phasor impedance at the excitation frequency f_x was estimated using

$$Z[n] = \frac{V[n]}{I[n]}, \tag{8}$$

where $V[n]$ is the discrete-time voltage phasor, estimated from the time signal using quadrature demodulation,

$$V[n] = \frac{1}{M}\sum_{m=0}^{M-1} v[m+nM]\exp\left(-\text{j}2\pi f_x\left(m+nM\right)\Delta t\right). \tag{9}$$

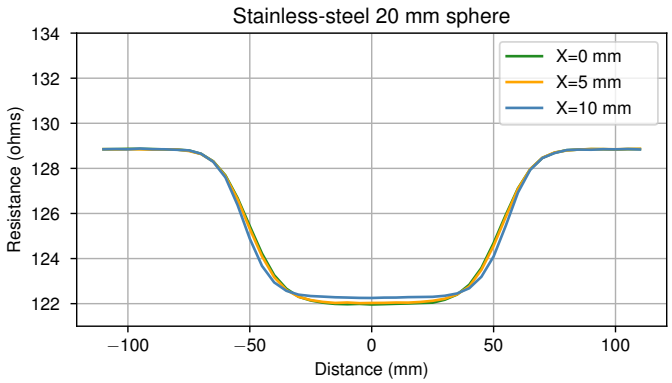

Fig. 7. Simulated resistance of a single sensor as a function of position for a 20 mm diameter stainless-steel sphere.

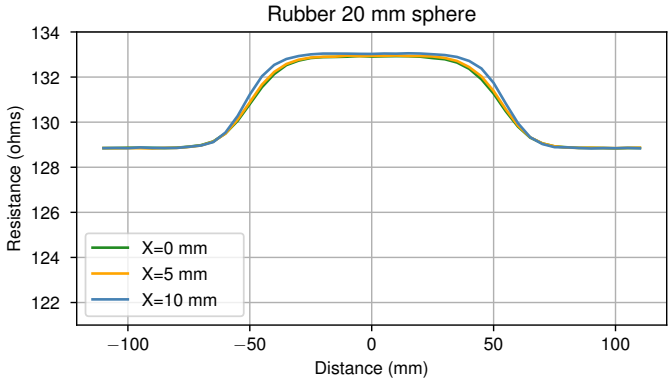

Fig. 8. Simulated resistance of a single sensor as a function of position for a 20 mm diameter insulating sphere.

Here M is the decimation factor and $v[n]$ is the discrete-time voltage signal. The discrete-time current phasor, $I[n]$, is estimated in the same way.

At 10 kHz, the imaginary part of the estimated impedance was neglible and was ignored. This is because the conduction current dominates the displacement current at low frequencies.

V. Results

The simulated results for conducting and insulating 20 mm diameter spheres are shown in Figure 7 and Figure 8. The results are plotted as a function of the radial position of the object with 0 mm being in the centre of the pipe. Similar results are shown in Figure 9 and Figure 10 for 10 mm diameter spheres.

The system was initially tested using conductive (stainless-steel) and insulating (stone) spheres of 20 mm and 19 mm diameters. A plot of the resistance as a function of time, estimated from the voltage and current measurements, is shown in Figure 15. Note how the resistance increases with the insulating foreign object and decreases with a conducting foreign object.

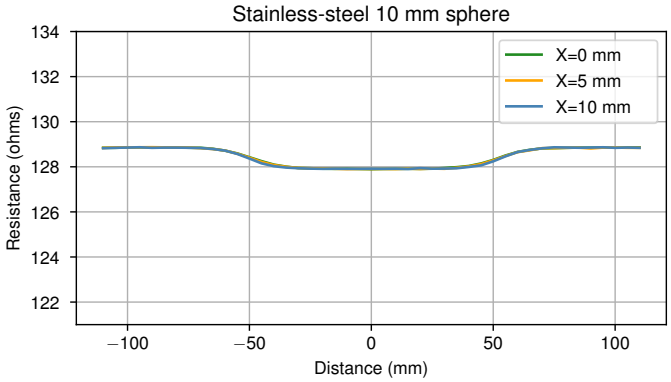

Fig. 9. Simulated resistance of a single sensor as a function of position for a 10 mm diameter stainless-steel sphere.

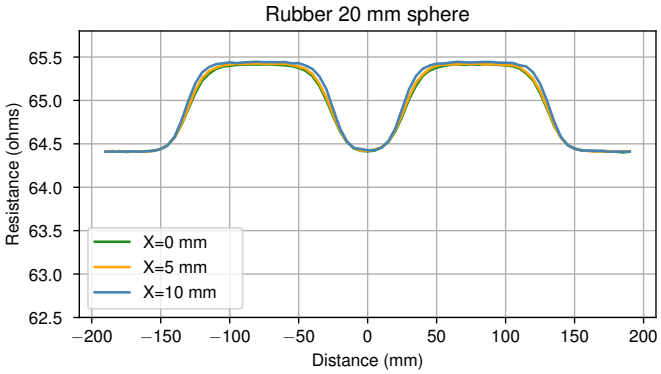

Fig. 12. Measured resistance change for a 20 mm diameter rubber sphere as a function of position for a dual sensor with single excitation.

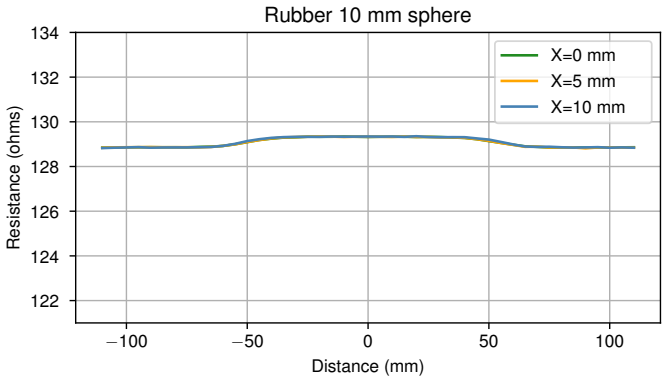

Fig. 10. Simulated resistance of a single sensor as a function of position for a 10 mm diameter insulating sphere.

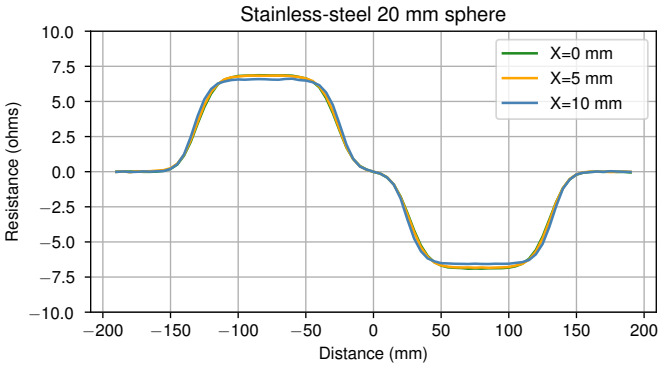

Fig. 13. Measured resistance for a 20 mm diameter stainless-steel sphere as a function of position for a dual sensor with dual excitation.

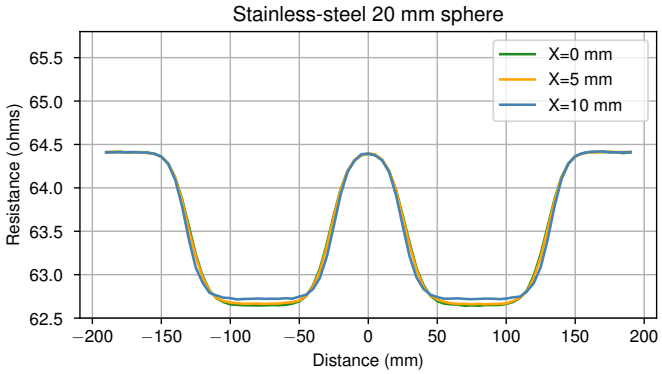

Fig. 11. Measured resistance change for a 20 mm diameter stainless-steel sphere as a function of position for a dual sensor with single excitation.

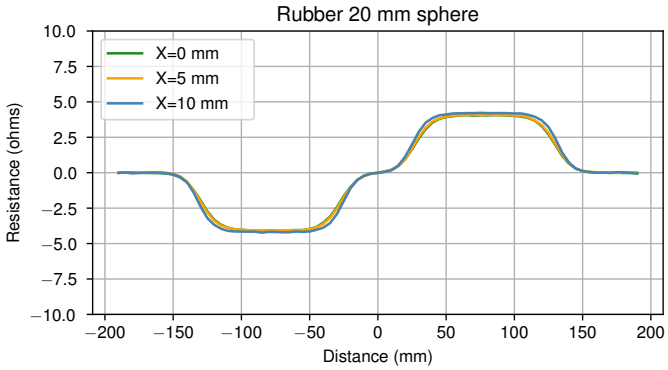

Fig. 14. Measured resistance for a 20 mm diameter rubber sphere as a function of position for a dual sensor with dual excitation.

VI. Discussion

The simulations show that the resistance drops for a conductive object (Figure 7) and increases for an insulating object (Figure 8). There is a small variation of resistance with the radial location of the object. As expected, a smaller object produces a smaller resistance change (Figure 9, Figure 10).

As shown in Figure 11 and Figure 12, the dual sensor with single excitation produces two deviations in measured resistance as a foreign object passes by. The first deviation is due to the object entering sensor 1 and the second deviation is due to the object entering sensor 2. The speed of the object can be found from the time-delay between the displacements. This can be estimated using autocorrelation.

The dual sensor with dual excitation also produces two deviations in measured resistance as a foreign object passes by, see Figure 14 and Figure 13. However, the second deviation has the opposite sign. This has the advantage that the resistance variation can be compensated due to changes in the fluid conductivity, say due to temperature changes. The speed of the object can also be found, using cross-correlation of the resistance signatures from the two sensors. The main disadvantage of dual excitation is that needs an additional insulating section of pipe to avoid shorting of the sources by grounding of the pipework.

There is a small discrepancy between the simulated and measured results due to differences in the conductivity of the medium, since this is a function of the medium temperature and salinity.

VII. Conclusion

The proposed system presents a simple way to reliably detect foreign objects within liquid food passing through foods. Further work is required to determine what is the smallest object that can be detected using change point detection for a given geometry of sight-glass and speed of object movement.

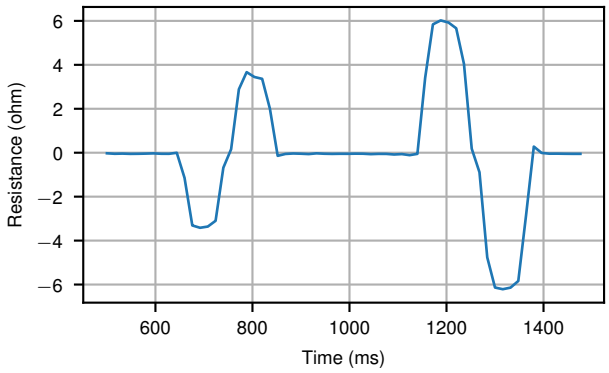

Fig. 15. Measured resistance difference for a 19 mm diameter stone (insulating) sphere, followed by a 20 mm diameter stainless-steel sphere, as a function of time for a dual sensor with dual excitation.

Acknowledgments

This work is funded by the New Zealand Ministry of Business, Innovation and Employment (MBIE) under the Endeavour fund. The authors would also like to thank the technical staff of Electrical and Computer Engineering department at the University of Canterbury for their invaluable assistance.

References

[1] M. T. M. Khairi, S. Ibrahim, M. A. M. Yunus, and A. R. Wahap, "Detection of foreign objects in milk using an ultrasonic system," *Indonesian Journal of Electrical Engineering and Computer Science*, vol. 15, no. 3, pp. 1241–1249, 2019.

[2] K. Payne, C. A. O'Bryan, J. A. Marcy, and P. G. Crandall, "Detection and prevention of foreign material in food: A review," *Heliyon*, vol. 9, no. 9, 2023.

[3] V. Mohammadi, M. Ghasemi-Varnamkhasti, R. Ebrahimi, and M. Abbasvali, "Ultrasonic techniques for the milk production industry," *Measurement*, vol. 58, pp. 93–102, 2014.

[4] A. Giacomozzi, J. Benedito, T. E. G. Álvarez-Arenas, and J. V. Garcia-Perez, "Air-coupled ultrasonic inspection of foods: A review," *IEEE Open Journal of Ultrasonics, Ferroelectrics, and Frequency Control*, 2024.

[5] R. P. Haff and N. Toyofuku, "X-ray detection of defects and contaminants in the food industry," *Sensing and Instrumentation for Food Quality and Safety*, vol. 2, pp. 262–273, 2008.

[6] M. Bech, O. Bunk, T. Donath, R. Feidenhans, C. David, and F. Pfeiffer, "Quantitative x-ray dark-field computed tomography," *Physics in Medicine & Biology*, vol. 55, no. 18, p. 5529, 2010.

[7] H. Einarsdóttir, M. J. Emerson, L. H. Clemmensen, K. Scherer, K. Willer, M. Bech, R. Larsen, B. K. Ersbøll, and F. Pfeiffer, "Novelty detection of foreign objects in food using multi-modal x-ray imaging," *Food control*, vol. 67, pp. 39–47, 2016.

[8] B. Alsaid, T. Saroufil, R. Berim, S. Majzoub, and A. J. Hussain, "Food physical contamination detection using ai-enhanced electrical impedance tomography," *IEEE Transactions on AgriFood Electronics*, 2024.

[9] Y. Wu, F. F. Hanzaee, D. Jiang, R. H. Bayford, and A. Demosthenous, "Electrical impedance tomography for biomedical applications: Circuits and systems review," *IEEE Open Journal of Circuits and Systems*, vol. 2, pp. 380–397, 2021.

[10] J. Zhu, B. Heffernan, M. Hayes, and S. Perry, "Electromagnetic detection of foreign bodies flowing in a pipe with continuous longitudinal electric field excitation," in *2024 IEEE International Instrumentation and Measurement Technology Conference (I2MTC)*. IEEE, 2024, pp. 1–6.

[11] B. Heffernan, M. Hayes, and M. Franks, "A smart electrode for heating and/or determining timber properties of logs," in *2024 IEEE International Instrumentation and Measurement Technology Conference (I2MTC)*. IEEE, 2024, pp. 1–6.